Letter

Gaspar Armelles*, Luca Bergamini, Nerea Zabala, María Ujué González, Fernando García, Raquel Alvaro, Javier Aizpurua and Alfonso Cebollada*

Broad band infrared modulation using spintronic-plasmonic metasurfaces

https://doi.org/10.1515/nanoph-2019-0183
Received June 18, 2019; revised July 19, 2019; accepted July 21, 2019

Abstract: We present magnetic field induced modulation of the optical response of slit plasmonic metasurfaces fabricated out of giant magnetoresistance/spintronic materials in the 2–17 μm spectral range of the spectrum. The modulation of the slit plasmonic modes is due to the modification of the electrical resistivity (and, in turn, of the optical constants) induced by the application of an external magnetic field. This modulation is found to continuously increase both with the slit concentration and with the slit resonance wavelength, with a prospective further increase for wavelengths of up to 60–80 μm. The direct fabrication and implementation of the modulation setup opens a competitive route for the development of active plasmonic metasurfaces in a wide spectral range.

Keywords: plasmonics; active metasurfaces; giant magnetoresistance (GMR); spintronics; slits.

1 Introduction

The concept of metasurface has emerged as a new approach to manipulate light using smartly designed, two-dimensional arrangements of subwavelength optical building blocks (scatterers) [1–4]. The capability of these structures to interact with light is determined basically by the intrinsic optical properties of the scatterer constituent materials, their size, shape, and spatial distribution. Focusing on the properties of the scatterers, one of the aspects which greatly expand the perspectives for practical applications of metasurfaces is their active character, based on the possibility to have in-hand additional degrees of freedom to control light via tunable or changing structures. This can be done for example by acting on the constituents material properties, as shown by several studies performed in the last years [5]. Different materials with great potential for active nanophotonic devices were already proposed and studied. For instance, magneto-optical metals such as Fe, Co, or Ni [6, 7], and ferroelectric materials such as $BaTiO_3$ [8, 9] and $LiNbO_3$ [10] were shown to change their permittivity tensor under the application of an external magnetic and electric DC field, respectively. Phase-change materials as VO_2 also exhibit a change in their optical response, namely an insulator-to-metal transition, which can be driven by either heating the sample or using external laser pump pulses [11]. This change in the permittivity can be exploited, among other uses, for increasing the sensitivity of optical sensors [12–15], creating switching mono/bi-directional devices [16, 17] or fabricating other active infrared devices [18–20]. Recently, the family of the giant magnetoresistance (GMR) materials is incorporated into the list of active-control opportunities, demonstrating modulation of mid-infrared response in spintronic-plasmonic platforms using very low magnetic fields [21, 22]. This new approach exploits the spin character of the conduction electrons via the spin-dependent electron transport properties of GMR metallic multilayers [23–25], merging, as a result, spintronic and plasmonics. This is due to the change in the optical response induced by the magnetic field as a result of the change in electrical resistivity (magnetorefractive effect or MRE) [26–27], which enables fast and contactless modulation of the optical properties of the spintronic material in the IR and longer wavelengths.

A key advantage of the GMR modulation mechanism is its usable spectral range. As the magnetic field induced change of the resistivity (Figure 1A) is linked to

***Corresponding authors: Gaspar Armelles and Alfonso Cebollada,** Instituto de Micro y Nanotecnología, IMN-CNM-CSIC, Isaac Newton, 8, Tres Cantos 28760, Madrid, Spain, e-mail: Gaspar.armelles@csic.es (G. Armelles); alfonso.cebollada@csic.es (A. Cebollada). https://orcid.org/0000-0002-2563-1621 (G. Armelles)
Luca Bergamini and Nerea Zabala: Materials Physics Center, CSIC-UPV/EHU and DIPC, San Sebastian 20018, Spain; and Department of Electricity and Electronics, FCT-ZTF, UPV-EHU, Bilbao 48080, Spain
María Ujué González, Fernando García and Raquel Alvaro: Instituto de Micro y Nanotecnología, IMN-CNM-CSIC, Isaac Newton, 8, Tres Cantos 28760, Madrid, Spain
Javier Aizpurua: Materials Physics Center, CSIC-UPV/EHU and DIPC, San Sebastian 20018, Spain

the conduction electrons, which are responsible for the optical properties of the GMR multilayer from the mid IR to nearly the DC limit, the same active material can potentially allow for a similar modulation mechanism in different spectral ranges (mid-far IR, THz, GHz…), by simply adapting the size and shape of the scatterers and their spatial distribution. In this work we experimentally demonstrate and theoretically confirm that plasmonic metasurfaces based on GMR magnetic multilayers show spintronic modulation of their optical properties in a very large spectral range, using very low magnetic fields, and with an increase of the optical modulation amplitude as we increase the wavelength. This opens an additional route for an active control of plasmonic platforms in a broad spectral range in the IR using materials and concepts well known in spintronics and easily transferable to nanophotonics.

2 Experimental

The metasurfaces that we consider in this work consist of different arrays of randomly arranged slits (the orientation of the slits is the same for all of them but their position within the array is random) fabricated on 70 nm thick $Ni_{81}Fe_{19}$/Au multilayers exhibiting 3.8% GMR [21, 28]. We used a random arrangement to avoid diffraction effects intrinsically linked to ordered structures and the

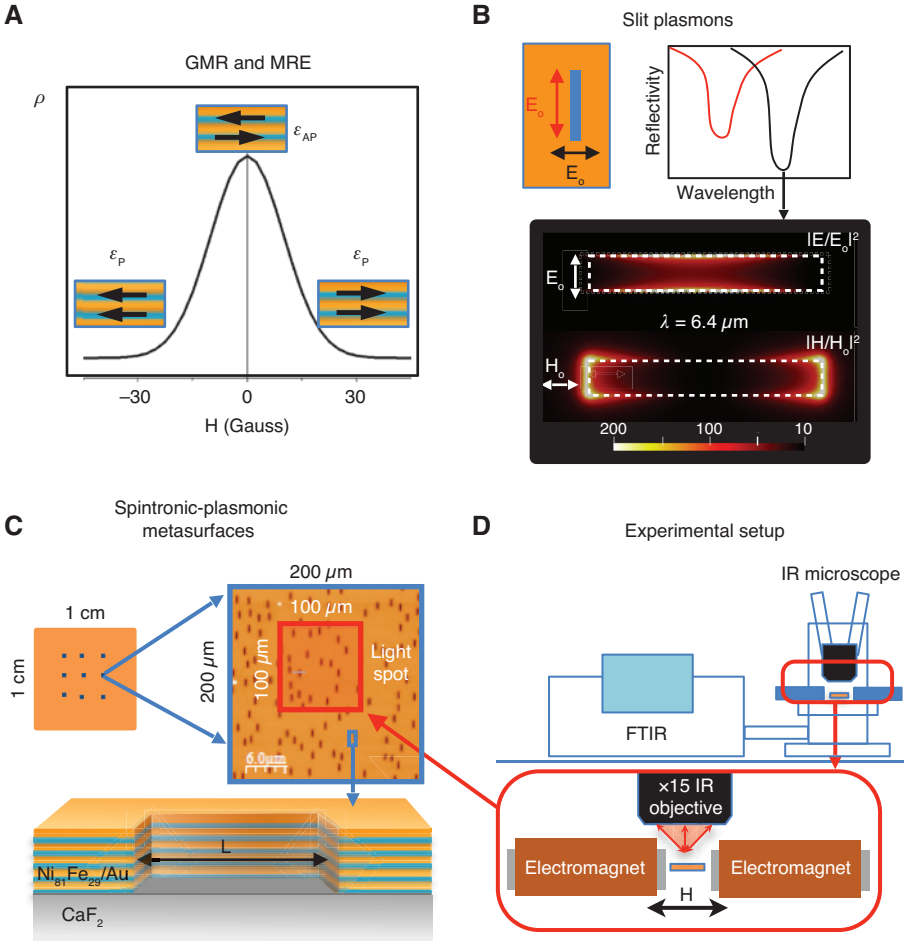

Figure 1: Modulation physical mechanism, selected resonant elements and experimental setup.
(A) In a giant magnetoresistance multilayer the magnetizations of the ferromagnetic layers can be switched from antiparallel (AP) to parallel (P) configuration by the application of a magnetic field. This produces a change in the electrical resistivity (ρ) and, therefore, a change in the dielectric constant ε (ε_{AP}, ε_{P}). (B) A slit in a continuous multilayer has longitudinal (red) and transverse (black) plasmon resonant modes. The near electromagnetic field enhancement reveals the longitudinal magnetic dipolar pattern for the transverse polarization of the exciting electric field. (C) By focused ion beam patterning techniques it is possible to fabricate a wide variety of slit arrays in a single 1 cm^2 sample. We have fabricated several 200 μm × 200 μm slit disordered arrays in a $Ni_{81}Fe_{21}$/Au multilayer with varying slit length and areal concentration. (D) Slit arrays are measured in a FTIR-IR microscope setup with a ferrite electromagnet in the near vicinity of the sample. Reflectivity and magnetic modulation of the reflectivity are measured in 100 μm × 100 μm areas of each array.

excitation of surface plasmon polaritons (propagating plasmons) mediated by the diffraction grating, and therefore to limit the spectral analysis to the localized optical response of the slits. The slits are characterized by resonant modes that can be excited with light polarized either parallel or perpendicular to the slit long axis, the perpendicular polarization mode (longitudinal mode) appearing at longer wavelengths than the parallel one (transverse mode) (Figure 1B). These longitudinal modes have a strong magnetic dipolar character, revealed by the near field distribution of the electromagnetic field at resonance (Figure 1B) [29, 30]. Moreover, the position of the perpendicular polarization mode can be easily tuned by changing the length of the slit [30, 31], a property exploited in the present work to explore the modulation capabilities of these metasurfaces in the 2–17 μm spectral range.

The slits random pattern was created with an algorithm that generated random positions for each individual slit and then excluded those positions that were closer than a certain predefined distance in order to avoid interaction effects. The arrays were fabricated by direct focused ion beam (FIB) milling from a $Ni_{81}Fe_{19}$/Au multilayer by simply removing the slit area off the continuous film. Following this method, a large variety of slit arrays with different sizes was easily and rapidly fabricated in a single step from a macroscopic single sample. In our case (Figure 1C), GMR $Ni_{81}Fe_{19}$/Au multilayers were grown on 1×1 cm^2 CaF_2 substrates and then several 200×200 μm^2 slit arrays were patterned in the central part of the sample. Slits 0.3 μm wide and with lengths varying between 1 μm and 5 μm in steps of 1 μm were fabricated in this way. The slit concentration was also varied between 1.4% and 3.7% (percentage of total surface occupied by the slits). This allows carrying out a systematic study on the slit sizes and concentration in a single 1×1 cm^2 multilayer with identical properties of the GMR material for all the arrays.

The optical characterization of the central 100×100 μm^2 area of each array was carried out using a Bruker Vertex 70 FTIR spectrometer (Bruker Optik, Ettlingen, Germany) with a coupled Hyperion microscope equipped with a reflecting $15\times$ Schwarzschild objective (Figure 1D). This objective has a 24 mm working distance and 0.4 numerical aperture. Light was polarized either along the long or short axis of the slits, referred to in the following as parallel and perpendicular polarization, respectively. The large working distance of the objective allows the insertion of the sample into a small ferrite electromagnet capable of applying a magnetic field large enough to observe the GMR effect in the material (detailed sketch shown in Figure 1D). As such, both reflectivity, and magnetic field induced changes in reflectivity for the different slit arrays were measured in the 2–17 μm spectral range.

3 Results and discussion

First we study the dependence of the reflectivity and its magnetic field modulation on the concentration of slits. In Figure 2A we show atomic force microscopy (AFM) images of three different samples, all of them slits of length 2 μm and width 0.3 μm, but fabricated with slit concentrations of 2.1%, 2.9%, and 3.7% in area. The random arrangement and gradual reduction of the average inter-slit distance as concentration increases can be clearly observed. In Figure 2B we present the corresponding experimental reflectivity spectra. For perpendicular polarization of the incident light (see Figure 1B) a clear dip is observed in the reflectivity spectrum, related to the excitation of the longitudinal mode of the slits. The intensity of the resonance dip increases with slit concentration, due to the increase in the number of resonant elements. Additionally, a very small blue shift of the resonance is observed with increasing slit concentration, suggesting a very small inter-slit interaction in this range of concentrations. In contrast, when incident light is polarized parallel to the slits, the reflectivity spectrum is featureless, with a monotonous decrease of the reflectivity as the wavelength is decreased (for clarity only the 2.1% spectrum is shown in the figure). The absence of any feature in the spectrum in such a situation is related to the width of the slit ($w = 0.3$ μm) which locates the spectral position of the transversal mode of the slit in a range not available in our experimental setup. The corresponding simulated spectra are also shown in Figure 2B. These concentration-dependent simulations of reflectivity (R) were performed with the use of COMSOL Multiphysics – COMSOL Server (Stockholm, Sweden) [32], and considering a distribution of slits to recreate the concentration of the measured samples (see Supporting Information for further details). As it can be observed, the agreement between theory and experiments is good, with somehow narrower and more intense dips obtained theoretically. As the magnetic modulation is concerned, in Figure 2C we show the normalized magnetic field induced reflectivity changes $\Delta R/R$, where ΔR is the difference in reflectivity between the high and low electrical resistivity states and R the reflectivity at zero field, as shown in Figure 1A. Like the reflectivity, the magnetic modulation also depends on the light polarization: for parallel polarization of the light the spectra of all the samples consist of a broad dip (only the 2.1% spectrum is shown for clarity). On the other hand, for perpendicular polarization of the incident light, we

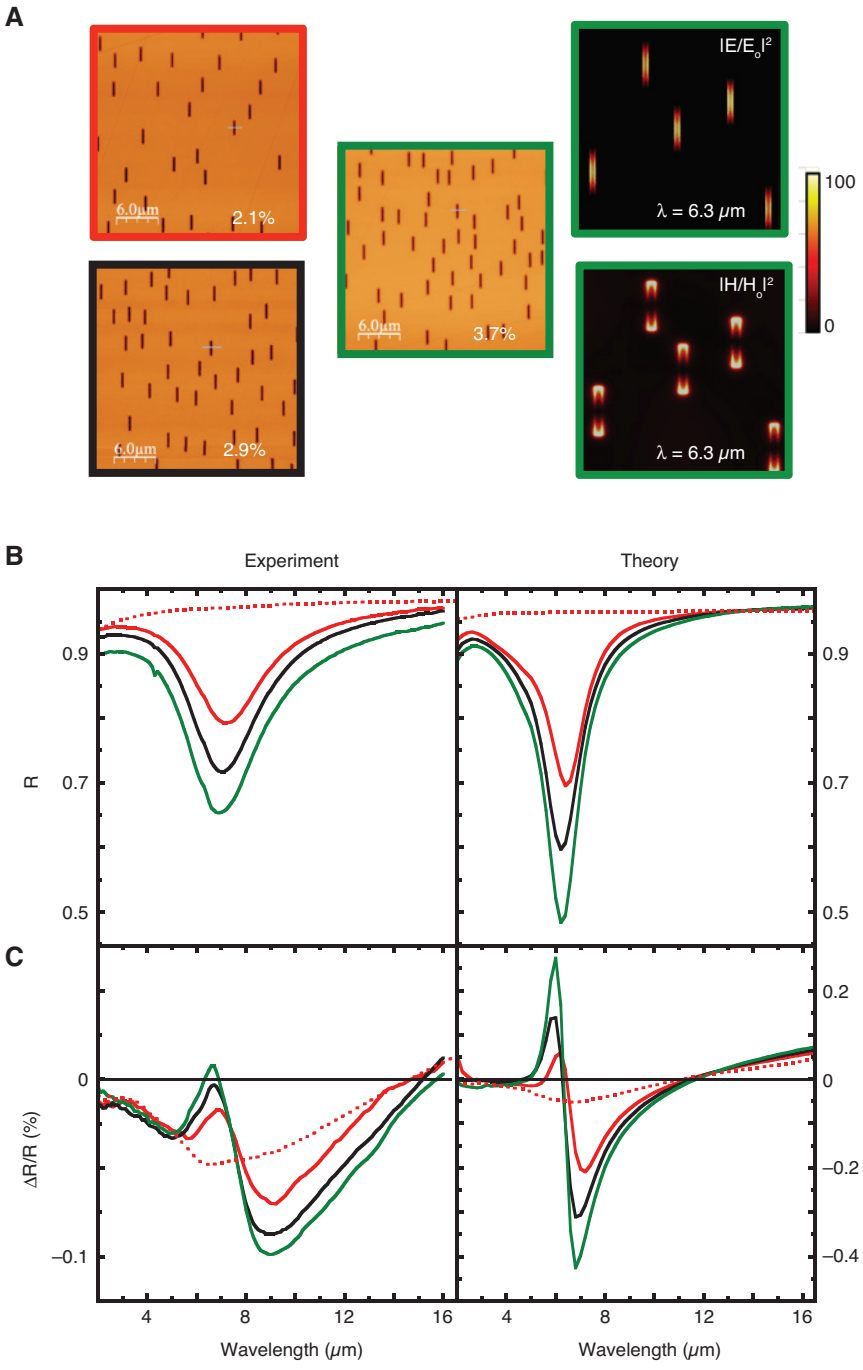

Figure 2: Dependence of the reflectivity and its magnetic field modulation on the concentration of slits.
(A) Atomic force microscopy images of the fabricated arrays for three different slits concentrations: 2.1% (red line), 2.9% (black line), and 3.7% (green line). The length of the slits is 2 microns. The electromagnetic field maps calculated for the sample of 3.7% slit concentration are shown on the right side. (B) Experimental (left) and theoretical (right) reflectivity (R) for the three slits arrays, for light polarized perpendicular (full lines) and parallel to the slit long axis (dotted line), respectively. (C) Magnetic modulation of the reflectivity (ΔR/R) for the three slits arrays of different concentrations, for perpendicularly polarized light (full lines) and parallelly polarized (dotted line), respectively.

observe a spectral structure with a derivative-like shape, which is linked to the modulation of the longitudinal slit mode, superimposed to the broad dip. The broad modulation dip for both polarizations is simply associated with the MRE for the $Ni_{81}Fe_{19}$/Au multilayer, whereas the derivative-like shape is associated with the magnetic modulation of the slit resonance, clearly indicating the antenna enhancing effect in the measured ΔR/R. As it can be observed, the

amplitude of this derivative-like feature is also concentration dependent, increasing as the concentration increases. Like in the R spectra, there is also a very small blue-shift as the slit concentration increases. Theoretical results are again in qualitative agreement with the experiments, though narrower and more intense features are obtained. The calculated near field maps for the different slit concentrations show very similar field enhancement patterns at resonance (right side of Figure 2A displays fields for 3.7% concentration). This confirms the small effect, for these concentrations, of interactions among close slits, which basically behave as independent resonant elements.

We next studied the dependence of the modulation on slit length. To this goal, a second series of slit arrays with slit concentration of 2.1% were fabricated, a concentration chosen to minimize the inter-slit interaction. In Figure 3A we show representative AFM images of this series. The complete set of optical experimental measurements and corresponding theoretical calculations for this series are displayed in Figure 3B,C, only for the perpendicular polarization of the incident light (results for the parallel polarization yield a featureless response, similar to the dotted curves in Figure 2B,C). Experimentally, neat reflectivity dips are observed for all slit lengths, with those corresponding to shorter slits appearing at lower wavelengths (Figure 3B, left). The positions of these dips are well described by effective antenna theory [30, 33–35] and correspond to the mode $n=1$. Moreover, the intensity of the dip gradually increases with slit length. These results are similar to those found in individual [30] and ordered arrays of slits [31] in an Au film. The side peaks which appear for the samples of $L=3$ μm, 4 μm, and 5 μm in the calculated spectra, and can be barely distinguished in the experimental spectra for the longest slit, correspond to the $n=3$ mode, but are not relevant for the present study. The corresponding measured magnetic modulation of the reflectivity for all slit lengths is shown in Figure 3C (left). As it can be seen, for all but the 1 μm long slits (which presents a broad modulation MRE like response), systematic derivative-like features are observed at the spectral position where the resonance peaks occur in the reflectivity spectra. These features appear convoluted with the broad modulation MRE band. Besides, the amplitude of these derivative-like features (I_{MR}) increases as the slit length is increased. As the selected concentration corresponds to an almost absent inter-slit interaction, this allows us to greatly simplify the theoretical part and consider a single slit. As it is observed in Figure 3B, the calculated slit length-dependent reflectivity is very similar to the experiment, with slightly narrower and more intense features as compared to the experiments. On the other hand, the calculated magnetic modulation spectra (Figure 3C) are qualitatively very similar to the experiments, but with larger amplitude [36].

This second set of results confirms that it is possible to control the intensity and spectral position of the magnetic modulation of the slit resonance via the slit length. The dependence of the resonance on the slit length is clearly summarized in Figure 4A. It is well known from plasmonic antenna theory [33–35] that the resonance wavelength is related to the antenna length by the scaling law $L \approx n\lambda_{eff}/2$, where λ_{eff} is an effective wavelength, L the antenna length, $n=1, 2, 3$ the mode order. From the resonance wavelength vs. slit length dependence (for the $n=1$ dipolar mode) summarized in Figure 4A, and considering the linear fit of the experimental results shown for the sample set studied, $\lambda_{eff}/\lambda \approx 0.79$, i.e. there is a 21% reduction of the resonance wavelength, which is in very good agreement with experiments performed in the infrared with lithographically fabricated solid antennas [37, 38]. This proves that the Babinet's principle is fulfilled in the antenna length scaling law.

In Figure 4B we plot the experimental (dots) and theoretical (squares) modulation amplitudes obtained for the different slit lengths, and therefore for different wavelengths. As observed, the modulation amplitude is basically zero for 4 μm wavelength (1 μm long slits) and gradually increases towards the far IR. This spectral dependence can be compared with the predicted spectral dependence of the modulation of the dielectric constant for these GMR multilayers [28]. This dependence is also shown as a continuous line in Figure 4B, with excellent agreement with the magnetic modulation of the slit resonance both in relative intensities and wavelength dependence over all the considered spectral range. This is a strong evidence of the modulation of the multilayers dielectric constant as the physical mechanism responsible for the modulation of the slit resonances, a mechanism that sets on in the mid IR, and appears less effective in the near IR and below. Thus, for the latter higher energy range, the classical magnetoplasmonic effect [39] that takes advantage of the magnetic modulation of the magneto-optical tensor components, instead of the optical constants, would be best suited for achieving an effective magnetoplasmonic modulation. Interestingly enough, the magnetic modulation of the dielectric constant of the system presented in this work can be extrapolated in the spectrum up to wavelengths of 90 μm (inset to Figure 4B), finding a continuous increase for longer wavelength, and approaching the GMR value limit at around 60–80 μm. For this particular sample, grown by sputtering, the GMR value is 3.8%, and it is limited by the presence of portions of the sample where the permalloy layers are ferromagnetically coupled, and do not contribute to

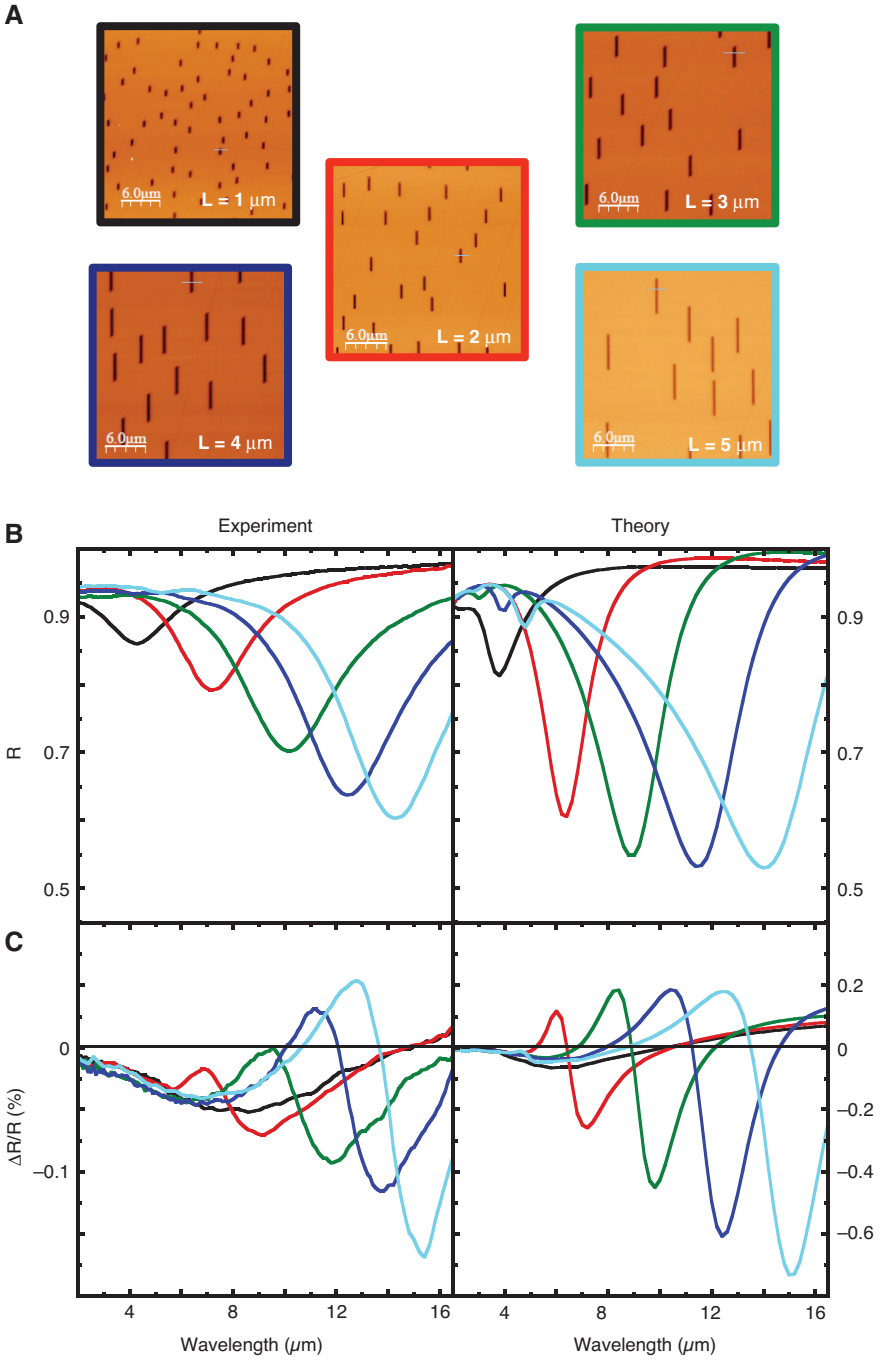

Figure 3: Dependence of the reflectivity and its magnetic field modulation on the slit length.
(A) Representative atomic force microscopy images of the slit arrays fabricated by FIB in a single 1×1 cm² $Ni_{81}Fe_{21}$/Au GMR multilayer for different slit lengths: black line 1 micron, red line 2 microns, green line 3 microns, blue line 4 microns, cyan line 5 microns. All the arrays have the same areal slit concentration (2.1% of the total area). (B) Experimental (left) and theoretical (right) reflectivity of the arrays. Light incidence is normal to the slits and with polarization perpendicular to the slit long axis. (C) Magnetic modulation of the reflectivity for the different arrays. I_{MR} represents the modulation intensity of the slit resonance.

the magnetoresistance. It shown that these regions can be reduced if the multilayer is grown by molecular beam epitaxy, reaching values of GMR at room temperature of 12%, very near of the theoretical estimation of 20% for the Py/Au system [25]. Exploring other materials systems with larger GMR values while maintaining low saturation magnetic fields is obviously a following step to take. This constitutes an exploratory roadmap on the feasibility of magnetic modulation of plasmonic metasurfaces towards the THz range. As it is based on a purely spintronic

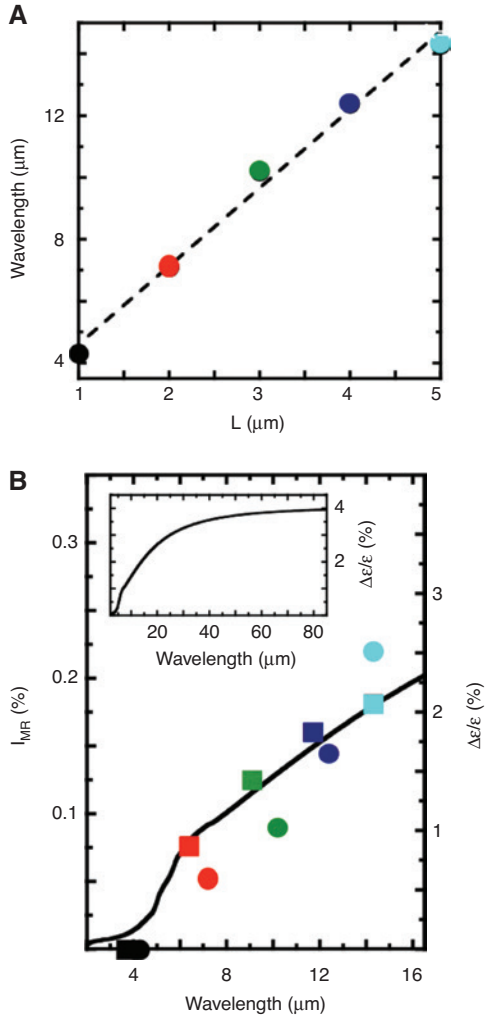

Figure 4: Wavelength dependence of magnetic modulation, with predicted continuous increase up to 90 microns.
(A) The position of the resonances for the different slit arrays studied in Figure 3 as a function of the slit length. (B) Amplitude of the experimental (dots) and theoretical, divided by 5, (squares) magnetic modulation (I_{MR}) of the slit resonance as a function of the slit resonance position. The black curve corresponds to the spectral dependence of the modulus of the relative magneto-induced variation of the dielectric constant, $\Delta\varepsilon/\varepsilon$ due to MRE. Inset: extrapolation of the spectral dependence, extended to 90 microns, of the ratio $\Delta\varepsilon/\varepsilon$.

mechanism, the modulation speeds are expected to be very fast and no electrical contacts are required. Here we have explored the use of a simple resonant scatterer, a slit, but obviously other shapes, distributions, and even different spintronic materials can be considered, widely extending the possibilities of this concept.

4 Conclusion

In this work we have fabricated a two-dimensional array of randomly distributed slits in a GMR $Ni_{81}Fe_{19}$/Au multilayer with different slit lengths. The structures present optical resonances whose positions depend on the slit length. Due to the MRE of the multilayers, we are able to modulate these resonances with very low magnetic fields, and to explore the spectral dependence of this magnetic modulation. We have found a continuous increase of the modulation of the electromagnetic response with both the slit concentration and the slit length. As the increase of slit length leads to a red-shift of the plasmon peak position at which the modulation takes on, this turns into an increase in the magnetic modulation when the spectral position of this modulation shifts towards the IR, which is predicted to increase even further for longer wavelengths. This result strongly suggests that GMR building blocks can be used to design active metasurfaces covering different spectral regions (mid-far IR, THz, GHz…), by simply adapting the size and shape of the building blocks and their spatial distribution. Besides, due to the intrinsic nature of the physical mechanism, a high speed modulation is expected without the needs of electrical contacts or complex designs.

Acknowledgments: We acknowledge financial support from MINECO through projects AMES (MAT 2014-58860-P), Quantum Spin Plasmonics (FIS2015-72035-EXP), Plasmo-Quanta (FIS2016-80174-P), MIRRAS (MAT2017-84009-R), and Comunidad de Madrid through project SINOXPHOS-CM (S2018/BAA-4403). LB, NZ, and JA acknowledge support from the Department of Education of the Basque Government under project IT1164-19, and the Department of Industry of the Basque Government under Elkartek project KK-2018/00001. We acknowledge the service from the MiNa Laboratory at IMN and funding from MINECO under project CSIC13-4E-1794 and from CM under project S2018/NMT-4291 TEC2SPACE, both with support from EU (FEDER, FSE).

References

[1] Kildishev AV, Boltasseva A, Shalaev VM. Planar photonics with metasurfaces. Science 2013;339:1232009.
[2] Yu N, Capasso F. Flat optics with designer metasurfaces. Nat Mater 2014;13:139.
[3] Chen HT, Taylor AJ, Yu N. A review of metasurfaces: physics and applications. Rep Prog Phys 2016;79:076401.
[4] Li A, Singh S, Sievenpiper D. Metasurfaces and their applications. Nanophoton 2018;7:989–1011.
[5] Choudhury SM, Wang D, Chaudhuri K, et al. Material platforms for optical metasurfaces. Nanophoton 2018;7:959–87.
[6] Ebert H. Magneto-optical effects in transition metal systems. Rep Prog Phys 1996;59:1665–735.

[7] Oppeneer P, Antonov V. Spin-orbit-influenced spectroscopies of magnetic solids. In: Ebert H, Schütz G, editors. Berlin: Springer, 1996:29.
[8] Zgonik M, Bernasconi P, Duelli M, et al. Dielectric, elastic, piezoelectric, electro-optic, and elasto-optic tensors of BaTioz crystals. Phys Rev B 1994;50:5941–9.
[9] Abel S, Stöferle T, Marchiori C, et al. A strong electro-optically active lead-free ferroelectric integrated on silicon. Nat Commun 2012;4:1671.
[10] Gupta MC, Ballato J. The handbook of photonics. 2nd ed, Boca Raton, FL, USA, CRC Press, 2019.
[11] Muskens OL, Bergamini L, Wang Y, et al. Antenna-assisted picosecond control of nanoscale phase transition in vanadium dioxide. Light Sci Appl 2016;5:e16173.
[12] Maccaferri N, Gregorczyk KE, de Oliveira TVAG, et al. Ultrasensitive and label-free molecular-level detection enabled by light phase control in magnetoplasmonic nanoantennas. Nat Commun 2015;6:6150.
[13] Ignatyeva DO, Knyazev GA, Kapralov PO, Dietler G, Sekatskii SK, Belotelov VI. Magneto-optical plasmonic heterostructure with ultranarrow resonance for sensing applications. Sci Rep 2016;6:28077.
[14] Knyazev G, Kapralov PO, Gusev NA, et al. Magnetoplasmonic crystals for highly sensitive magnetometry. ACS Photon 2018;5:4951–9.
[15] Pourjamal S, Kataja M, Maccaferri N, Vavassori P, Van Dijken S. Hybrid Ni/SiO_2/Au dimer arrays for high-resolution refractive index sensing. Nanophoton 2018;7:905–12.
[16] Davoyan A, Engheta N. Electrically controlled one-way photon flow in plasmonic nanostructures. Nat Commun 2014;5:5250.
[17] Shimizu H, Zayets V. Plasmonic isolator for photonic integrated circuits. MRS Bulletin 2018;43:425.
[18] Xiong C, Pernice WHP, Ngai JH, et al. Active silicon integrated nanophotonics: ferroelectric $BaTiO_3$ devices. Nano Lett 2014;14:1419–25.
[19] Beechem T, Goldflam MD, Sinclair MB, et al. Tunable infrared devices via ferroelectric domain reconfiguration. Adv Opt Mater 2018;6:1800862.
[20] Dong W, Qiu Y, Zhou X, et al. Tunable mid-infrared phase-change metasurface. Adv Opt Mater 2018;6:1701346.
[21] Armelles G, Cebollada A, García F, Pecharromán C. Magnetic modulation of mid-infrared plasmons using giant magnetoresistance. Opt Exp 2017;25:18784–96.
[22] Armelles G, Bergamini L, Zabala N, et al. Metamaterial platforms for spintronic modulation of mid-Infrared response under very weak magnetic field. ACS Photon 2018;5:3956–91.
[23] Baibich MN, Broto JM, Fert A, et al. Giant magnetoresistance of (001)Fe/(001)Cr magnetic superlattices. Phys Rev Lett 1988;61:2472–5.
[24] Binasch G, Grünberg P, Saurenbach F, Zinn W. Enhanced magnetoresistance in layered magnetic structures with antiferromagnetic interlayer exchange. Phys Rev B 1989;39:4828–30.
[25] Parkin SSP, Farrow RFC, Marks RF, Cebollada A, Harp GR, Savoy RJ. Oscillations of interlayer exchange coupling and giant magnetoresistance in (111) oriented permalloy/Au multilayers. Phys Rev Lett 1994;72:3718–21.
[26] Jacquet JC, Valet TA. A new magnetooptical effect discovered on magnetic multilayers: the magnetorefractive effect. Mat Res Soc Symp Proc 1995;384:477–90.
[27] Jin Z, Tkach A, Casper F, et al. Accessing the fundamentals of magnetotransport in metals with terahertz probes. Nat Phys 2015;11:761–6.
[28] Armelles G, Cebollada A, García F. Au dependence of the mid infrared optical and magnetorefractive properties of Ni81Fe19/Au GMR multilayers. Opt Mat Exp 2019;9:923–31.
[29] Sepúlveda B, Alaverdyan Y, Alegret J, Käll M, Johansson P. Shape effects in the localized plasmon resonance of single nanoholes in thin metal films. Opt Exp 2008;14:5609–16.
[30] Yang HU, Olmon RL, Deryckx KS, et al. Accessing the optical magnetic near-field through Babinet's principle. ACS Photon 2014;1:894–9.
[31] Huck C, Vogt J, Sendner M, Hengstler D, Neubrech F, Pucci A. Plasmonic enhancement of infrared vibrational signals: nanoslits vs nanorods. ACS Photon 2015;2:1489–97.
[32] COMSOL Inc., COMSOL Multiphysics. https://www.comsol.com.
[33] Novotny L. Effective wavelength scaling for optical antenna. Phys Rev Lett 2007;98:266802–1–4.
[34] Bryant GW, García de Abajo FJ, Aizpurua J. Mapping the plasmon resonances of metallic nanoantennas. Nano Lett 2008;8:631–6.
[35] Neubrech F, Pucci A, Cornelius TW, Karim S, García-Etxarri A, Aizpurua J. Resonant plasmonic and vibrational coupling in a tailored nanoantenna for infrared detection. Phys Rev Lett 2008;101:157403–1–4.
[36] The intensity discrepancies between theory and experiments found here and in the previous part of this work are very likely due to the fact that the optical constants used for the calculations are those of unpatterned continuous multilayers. Fabrication induced roughness or magnetically dead edge regions due to Ga ion implantation in the FIB etching process may cause the actual modulation of the optical constants, especially in the slit surrounding area, to be smaller than those for the unpatterned film, with a reduction of the experimentally observed effects.
[37] Fumeaux C, Gritz MA, Codreanu I, Schaich WL, González FJ, Boreman GD. Measurement of the resonant lengths of infrared dipole antennas. Infrared Phys Technol 2000;41:271–81.
[38] Neubrech F, Weber D, Lovrincic R, et al. Resonances of individual metal nanowires in the infrared. Appl Phys Lett 2006;89:253104–1–3.
[39] Armelles G, Cebollada A, García-Martín A, González MU. Magnetoplasmonics: combining magnetic and plasmonic functionalities. Adv Opt Mater 2013;1:10–35.

Supplementary Material: The online version of this article offers supplementary material (https://doi.org/10.1515/nanoph-2019-0183).